Real-time studies of gallium adsorption and desorption kinetics on sapphire (0001) by grazing incidence small-angle x-ray scattering and x-ray fluorescence

Yiyi Wang, Ahmet S. Özcan, Karl F. Ludwig, and Anirban Bhattacharyya

Citation: Journal of Applied Physics **103**, 103538 (2008); doi: 10.1063/1.2936969
View online: http://dx.doi.org/10.1063/1.2936969
View Table of Contents: http://scitation.aip.org/content/aip/journal/jap/103/10?ver=pdfcov
Published by the AIP Publishing

Real-time studies of gallium adsorption and desorption kinetics on sapphire (0001) by grazing incidence small-angle x-ray scattering and x-ray fluorescence

Yiyi Wang,[1,a)] Ahmet S. Özcan,[1,b)] Karl F. Ludwig,[1] and Anirban Bhattacharyya[2]
[1]*Physics Department, Boston University, Boston, Massachusetts 02215, USA*
[2]*Department of Electrical and Computer Engineering, Boston University, Boston, Massachusetts 02215, USA*

(Received 3 October 2007; accepted 28 March 2008; published online 30 May 2008)

Gallium adsorption and desorption on *c*-plane sapphire has been studied by real-time grazing incidence small-angle x-ray scattering and x-ray fluorescence as a function of substrate temperature (680–740 °C) and Ga flux. The x-ray techniques monitor the surface morphology evolution and amount of Ga on the surface. During deposition, nanodroplets of liquid Ga are observed to form on the surface and coarsen. The growth of droplet size during continuous deposition follows dynamical scaling, in agreement with expectations from theory and simulations which include deposition-induced droplet coalescence. However, observation of continued droplet distance scale coarsening during desorption points to the necessity of including further physical processes in the modeling. The desorption rate at different substrate temperatures gives the activation energy of Ga desorption as 2.7 eV, comparable to measured activation energies for desorption from Ga droplets on other substrates and to the Ga heat of vaporization. © *2008 American Institute of Physics*. [DOI: 10.1063/1.2936969]

I. INTRODUCTION

Wide-bandgap III-V nitrides, such as GaN and its alloys, have important applications in optoelectronics and high-power devices. One of the commonly employed methods for growing GaN thin films is molecular beam epitaxy (MBE). The MBE technique utilizes effusion cells as metal sources and a reactive gas or a plasma source as the nitrogen source. Because of the lack of lattice matched substrates, GaN thin films are most commonly grown on sapphire, which has a good crystalline quality and relatively low cost.

One of the most important growth parameters that controls the properties of GaN films is the metal/nitrogen atomic flux ratio.[1–3] GaN deposition is typically performed under metal-rich conditions, which produces better quality and smoother films. Previous studies[1–4] have shown that during Ga-rich growth, under certain conditions, a liquid Ga adlayer forms on the surface. This Ga adlayer acts as an autosurfactant and enhances the migration of N atoms on the surface. Also, films grown in both Ga-polar and N-polar orientations are known to be stably terminated by Ga atoms. However, very high Ga/N atomic flux ratios and/or low substrate temperatures during growth typically cause macroscopic Ga droplet formation on the surface due to excess Ga. All these results suggest that the Ga adatoms play a very important role in the epitaxial growth of GaN films.

Because of the technological motivations for growing good quality GaN films, studies of Ga adsorption and desorption have been carried out on different surfaces using reflection high-energy electron diffraction (RHEED) and mass spectroscopy.[5–10] Although these techniques provide important information on the rates of Ga adsorption and desorption, they do not monitor the evolution of the surface morphology. Our recent study[11] of Ga adsorption and desorption presents information on surface morphology evolution during formation of Ga nanodroplets on sapphire and GaN surfaces by real-time surface-sensitive grazing incidence small-angle x-ray scattering (GISAXS). GISAXS is sensitive to the nanometer-size morphological changes on the surface, such as roughening and island formations.[12] Typically, GISAXS measurements can monitor lateral length scales between 1 and 250 nm at the surface. In this paper, a more complete series of Ga on sapphire samples were studied as a function of Ga deposition rate and substrate temperature by real-time GISAXS to monitor the surface morphology evolution. In addition, the Ga *K*-edge x-ray fluorescence, which

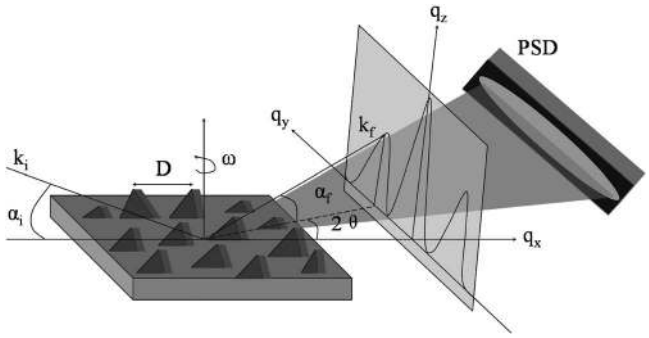

FIG. 1. Schematic of the x-ray grazing incidence diffraction geometry. Wavevectors $\mathbf{k}_i$ and $\mathbf{k}_f$ are the incident and scattered wave vectors, respectively. The linear position-sensitive detector is oriented parallel to the sample surface.

[a)]Author to whom correspondence should be addressed. Electronic mail: yiyiwang@buphy.bu.edu.
[b)]Currently at IBM Microelectronics, East Fishkill, NY.

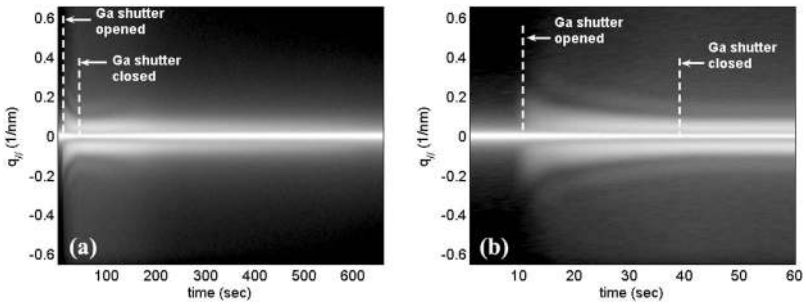

FIG. 2. The real-time GISAXS evolution on sapphire substrate at substrate temperature 720 °C and Ga cell temperature of 1050 °C (a) during Ga adsorption and desorption and (b) initial 30 s of Ga deposition.

is proportional to the number of Ga atoms on the surface, was measured to monitor the rates of Ga adsorption and desorption.

II. EXPERIMENTS

The Ga adsorption and desorption experiments were performed in a custom-made ultrahigh vacuum (UHV) x-ray diffraction chamber with a base pressure of 10^{-9} Torr installed at beamline X21 of National Synchrotron Light Source (NSLS) at Brookhaven National Laboratory (BNL). The *c*-plane sapphire substrates were small cuts from "epitaxial" quality commercial wafers. A dual filament Applied Epi SUMO effusion cell was employed for Ga deposition. During Ga adsorption/desorption studies the sample temperature was monitored by a pyrometer and a thermocouple at the back of the sample heater. Prior to the Ga adsorption experiments, the samples were degassed by annealing in UHV at 800 °C for at least 30 min. RHEED analysis was performed to confirm the orientation and the smoothness of the starting surface.

An incident photon energy was chosen at 10.40 keV (above the Ga $K\alpha$ edge) with a flux of 2×10^{12} photons per second using a nondispersive Si (111) double-crystal monochromator with a beam size of 0.5×0.5 mm^2 at a storage ring current of 300 mA. For the real-time x-ray fluorescence experiment of Ga adsorption and desorption, the incidence angle was kept at 2°, while the exit angle was kept at 8°, away from the elastic scattering condition, to avoid the elastic scattering signals. The fluorescence signal of Ga $K\alpha$ was collected by a one-dimensional (1D) position sensitive detector (PSD) with 1 s time resolution mounted parallel to the sample surface.

The GISAXS geometry used in our experiments is shown in Fig. 1. The incidence angle was kept constant at 1°, while the exit angle was near the critical angle (0.2°) to the sample surface to enhance surface sensitivity. This geometry gives $q_z=0.9$ nm^{-1} (momentum transfer perpendicular to the surface). The asymmetric scattering geometry is chosen to avoid going directly through the specular rod itself—instead the GISAXS passes through the tail of the specular rod and $q_\parallel$ the momentum transfer parallel to the surface, can be small (0.005 nm^{-1}), but is never zero. We will refer to the GISAXS peak near $q_\parallel=0$ as the "near-specular" peak. For small surface roughness σ such that $q_z\sigma\ll1$, the GISAXS intensity is proportional to the surface structure factor, i.e., the square of the Fourier Transform of the height-height correlation function.[12]

III. RESULTS

A. GISAXS studies of surface morphology development during adsorption and desorption

1. General features

Figure 2(a) shows typical GISAXS time evolution during Ga adsorption and desorption. The sapphire substrate temperature was a constant 720 °C throughout the process. The Ga cell temperature was 1050 °C and the total exposure of Ga was 30 s for the data shown in Fig. 2. Initially, the scattering profile shows only the intensity of the near-specular reflection (at $q_\parallel\approx0$) from the sapphire substrate surface. As soon as the Ga shutter is opened, the diffuse scattering intensity increases immediately. Two kinds of peaks appear symmetrically on each side of the central peak after a few seconds. The positions of the high intensity peaks at low-$|q_\parallel|$ value, which we call the correlation peaks, are related to the distance between laterally correlated Ga droplets. The positions of lower intensity peaks at higher-$|q_\parallel|$ value, which we call the form factor peaks, are related to the size of Ga droplets. That is, they are the peaks associated with the internal structure and shape of the droplets. This observation suggests that the droplets are relatively uniform in lateral size. Figure 2(b) zooms in the initial 30 s Ga deposition, in which we can clearly see that both the correlation and form

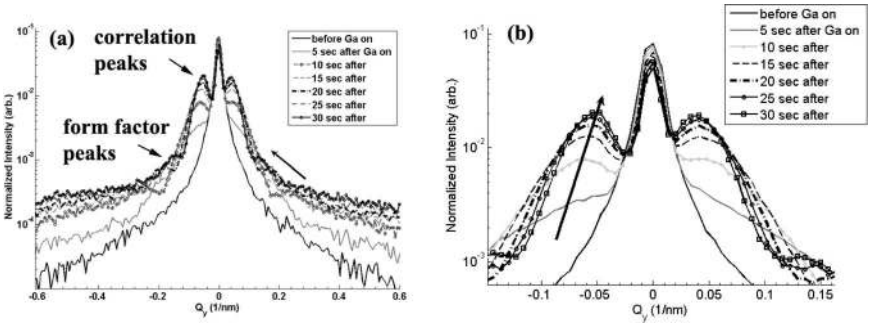

FIG. 3. (a) Selected slices from Fig. 2(b) of the real-time GISAXS evolution during Ga adsorption. (b) Zoomed-in region of correlation peaks at low $q_\parallel$.

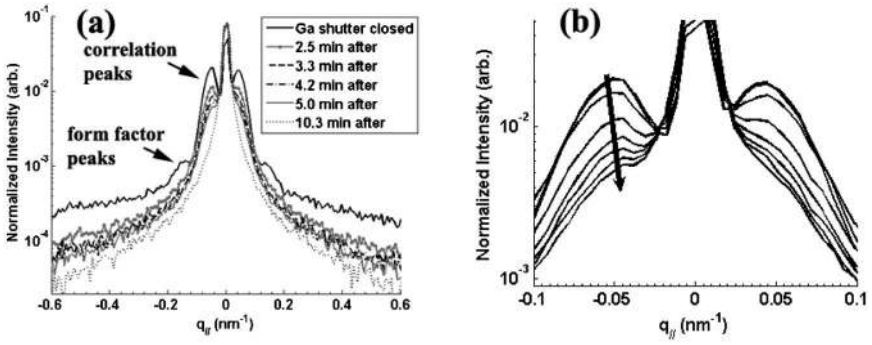

FIG. 4. (a) Selected slices from Fig. 2(a) of the real-time GISAXS evolution during Ga desorption. (b) Zoomed-in region of correlation peaks at low $q_{\|}$.

factor peaks grew and shifted towards smaller $|q_{\|}|$ value during Ga deposition. The increase in form factor peak intensity and shift of the peak position to lower wavenumber with time suggests the improvement of droplet uniformity and growth in droplet size. Similarly, the behavior of the correlation peaks suggests the improvement of correlation in the lateral direction and an increase in the lateral correlation length.

These observations can be seen more clearly in Fig. 3, which shows snapshots from Fig. 2(b) of the GISAXS time evolution during Ga adsorption. Figures 4(a) and 4(b) show that both kinds of peaks continued to evolve with further coarsening after the Ga shutter was closed (indicated by the arrows), but at a much slower rate than during Ga deposition. The peak position after 30 s of Ga deposition indicates the interdroplet distance is $2\pi/q_{\|\max} \sim 135$ nm. The droplet density calculated from the interdroplet distance is $\sim 5.5 \times 10^9/\mathrm{cm}^{-2}$. The relationship between droplet form factor peak position and average droplet size will vary slightly depending upon the droplet size distirubution and droplet shapes. Post-facto AFM and TEM studies discussed below show that the nitridated droplets are relatively flat. For simplicity, we therefore assume that the square of the droplet form factor is approximately that of a flat circular disk—i.e., the Airy function. In this case, the disk diameter is related to the position of the form factor peak maximum as $d \approx 3.27\pi/q_{\text{form factormax}}$.[13] The final position of the droplet form factor peak suggests that the average dot diameter is ~ 36 nm.

The desorption of Ga from the sapphire surface was essentially completed ~ 70 min after the Ga shutter closed. Figure 4(a) shows snapshots from Fig. 2(a) of the GISAXS time evolution during Ga desorption. Figure 4(b) shows the zoomed-in part of the correlation peak, which indicates the continued coarsening of the droplets during Ga desorption.

2. Surface morphology development during adsorption—scaling analysis

Figure 5 shows the GISAXS time evolution during continuous Ga deposition on *c*-plane sapphire at Ga cell temperature 1020 °C and substrate temperature 580 °C. The symmetric peaks which appeared initially at $|q_{\|}| \sim 0.2$ nm^{-1} moved inwards during deposition due to the coarsening of Ga droplets. The theory of droplet formation proposed by Family and Meakin[14] predicts a scaling behavior of the droplet size growth,

$$R(t) = t^{z/D}, \tag{1}$$

where R is the mean droplet size, z is a scaling exponent, and D is the droplet dimensionality. The exponent z depends on D: $z = D/(D-2)$ with the assumption of droplets forming on a two-dimensional substrate. The evolution of the interdroplet distance is easier to measure accurately from the data than the droplet size itself. We therefore assume that the droplet size is proportional to the interdroplet distance and plot instead the interdroplet distance as a function of deposition time in Fig. 6. The data can be fit well by a power law, which gives $z/D = 1.7$. According to the relationship between z and D, we calculate D to be ~ 2.6. This falls between the limits expected for two- and three-dimensional growth, consistent with the relatively flat droplets observed with AFM upon subsequent droplet nitridation.[11,15]

Family and Meakin also suggest that the distribution of droplet sizes during coarsening exhibits dynamic scaling. This would result in dynamic scaling of the GISAXS intensity evolution,

$$I(q_{\|},t) = I_{\max}(t) F\left(\frac{q_{\|}}{q_{\|\max}(t)}\right). \tag{2}$$

Figures 7(a) and 7(b) show the GISAXS plots during continuous Ga deposition every 5 s before and after scaling $q_{\|}$ and I values. The peak shapes at different times are almost

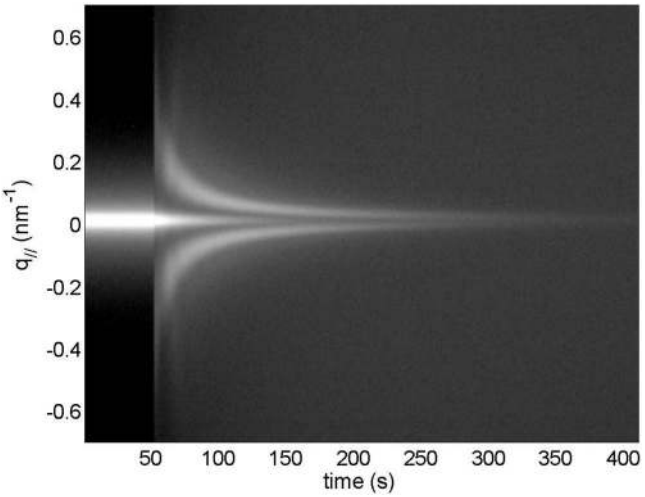

FIG. 5. GISAXS time evolution during continuous Ga deposition on *c*-plane sapphire at Ga cell temperature of 1020 °C and substrate temperature of 580 °C.

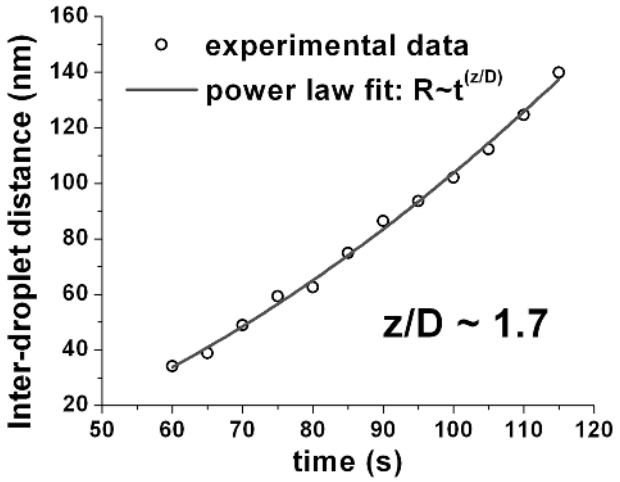

FIG. 6. (Color online) Plot of interdroplet distance as a function of Ga deposition time. Solid line represents the power law fitting.

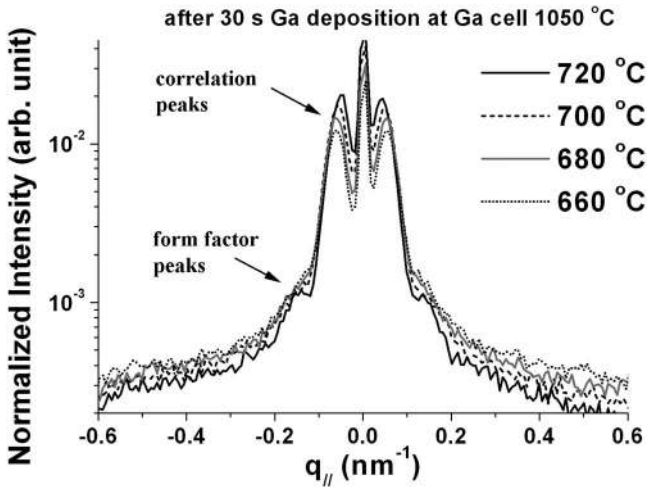

FIG. 8. GISAXS profile of four samples at different substrate temperatures after 30 s of Ga deposition at Ga effusion cell temperature of 1050 °C.

identical after the scaling, as shown in Fig. 7(b), consistent with the scaling behavior of the droplet growth proposed by Family and Meakin.[14]

3. Effect of substrate temperature and Ga flux on surface morphology development

Figure 8 shows the GISAXS profiles for different substrate temperatures when the Ga shutter was closed after 30 s of Ga deposition for four different substrate temperatures at a common Ga cell temperature of 1050 °C. The correlation peaks of the highest substrate temperature sample appear at the lowest $|q_{\|}|$ value. The lateral correlation length (interdroplet distance), the droplet density, and the droplet size calculated from those peaks are listed in Table I.

Figure 9 shows the GISAXS profile of four samples when the Ga shutter was closed after 30 s of Ga deposition at the same substrate temperature (720 °C) but different Ga cell temperatures, and hence, different Ga deposition rates and resulting thicknesses. The correlation peaks of the highest Ga cell temperature sample appear at the highest $|q_{\|}|$ value. The form factor peaks of the highest Ga cell temperature sample appear at the lowest $|q_{\|}|$ value and have the highest intensity. The peaks of the curve at Ga cell temperature 1005 °C cannot be distinguished clearly after 30 s Ga exposure, which might suggest that either the Ga droplets formed are not correlated or that the correlation length of the Ga droplets is beyond the range of GISAXS scans.

The lateral correlation length (interdroplet distance), the droplet density, and the droplet size calculated from those peaks are listed in Table II. The droplet information from GISAXS data listed in both tables indicates that, for a given deposition time, the droplet size and interdroplet distance depend on both the substrate temperature and the Ga flux. Our interpretation is that, in the Ga droplet regime at high substrate temperature, the high Ga evaporation rate causes the average droplet size to be relatively small, but the low net adsorption rate and high surface mobility give a relatively large distance between dots. Thus the droplet density is low. For a given substrate temperature, higher deposition rates give higher droplet density and larger droplet size.

B. Fluorescence studies of Ga adsoprtion/desorption kinetics

1. Kinetics as a function of Ga flux

Figure 10(a) shows the real-time Ga *K* fluorescence data during Ga adsorption and desorption at various Ga effusion cell temperatures. The substrate temperature was the same for all samples—a constant 700 °C. Figure 10(b) zooms in the initial Ga deposition of 60 s. The Ga effusion cell shutter was opened approximately 10 s after each scan started to obtain a base line for the scattering signals. The x-ray Ga *K* fluorescence intensity, which is proportional to the Ga amount on the surface, increased immediately after the surface was exposed to Ga.

Although the initial absorption curves show nonlinear growth, overall the adsorption process in these time regimes can be fit by a linear function with increasing slope at higher

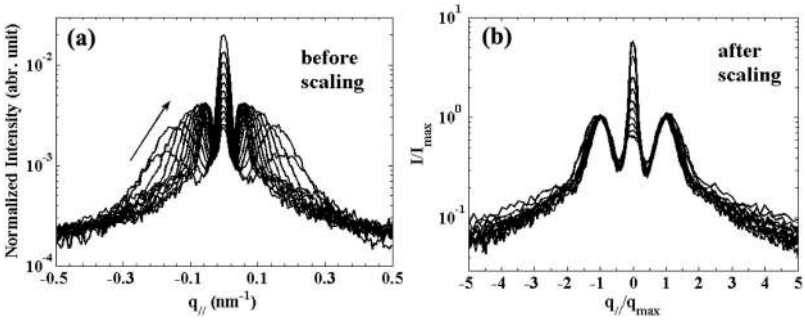

FIG. 7. GISAXS plots during continuous Ga deposition every 5 s on *c*-plane sapphire at Ga cell temperature of 1020 °C and substrate temperature of 580 °C before (a) and after (b) scaling $q_{\|}$ and *I* values.

TABLE I. Table of droplet distance, density, and size after 30 s deposition for Ga effusion cell temperature of 1050 °C.

Substrate temperature (°C)	Inter-droplet distance (nm)	Droplet density ($1/cm^2$)	Droplet size (nm)
720	135	5.5×10^{-9}	36.0
700	122	6.7×10^{-9}	37.6
680	113	7.8×10^{-9}	38.3
660	105	9.1×10^{-9}	39.2

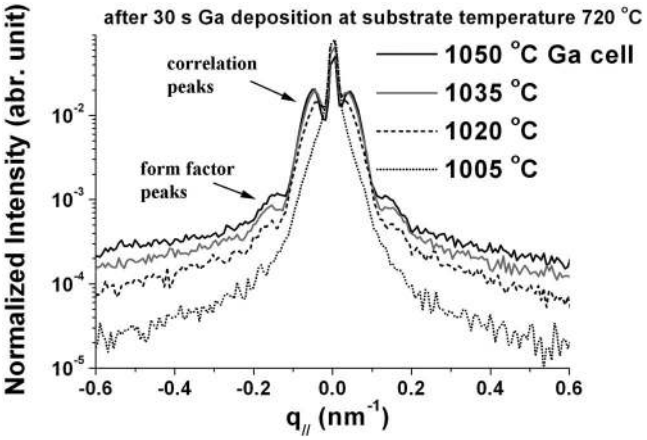

FIG. 9. GISAXS profile of four samples at different Ga effusion cell temperatures after 30 s of Ga deposition at substrate temperature of 720 °C.

TABLE II. Table of droplet distance, density, and size after 30 s deposition at substrate temperature 720 °C.

Ga cell temperature (°C)	Inter-droplet distance (nm)	Droplet density ($1/cm^2$)	Droplet size (nm)
1050	135	5.5×10^{-9}	36.0
1035	151	4.4×10^{-9}	34.6
1020	167	3.6×10^{-9}	32.8
1005	NA	NA	NA

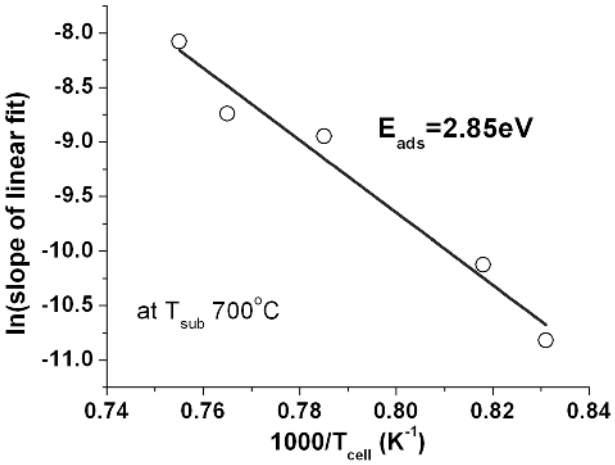

FIG. 11. (Color online) Plot of adsorption rates from linear fits as a function of Ga cell temperature.

Ga effusion cell temperature (i.e., higher Ga flux). It is perhaps surprising that, following the initial transient, the adsorption rate is approximately constant. In general we would expect that the net adsorption rate $A(t)$ at any time would be:

$$A(t) = F\alpha(t) - D(t), \tag{3}$$

where F is the incident flux of Ga (proportional to the vapor pressure of Ga in the effusion cell), $\alpha(t)$ is the time-dependent sticking coefficient, and $D(t)$ is the time-dependent desorption rate. Both the sticking coefficient and desorption rate could vary with time due to changes in surface coverage and morphology. In fact, the graphs show that desorption is significantly slower than adsorption in this regime and to a first approximation can be neglected. Beyond the initial nonlinear transient, the near linearity of the adsorption curves then implies that in this regime the sticking coefficient α is approximately constant in time.

An Arrhenius plot of the net adsorption rate as a function of the effusion cell temperature is shown in Fig. 11. The activation energy of the adsorption with changing effusion cell temperature is determined to be approximately 2.85 eV, which is in good agreement with the reported heat of Ga evaporation from the liquid, 2.5 eV,[16] as expected.

The desorption curves are complex. As the GISAXS results show, the surface morphology changes with time and we might therefore expect the temporal dependence of the desorption process to be complicated. Nonetheless, the fluorescence data during Ga desorption can be approximately fit

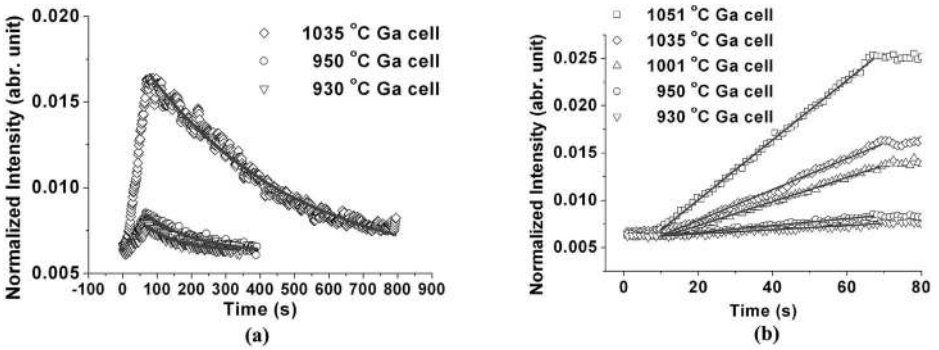

FIG. 10. Real-time Ga $K\alpha$ fluorescence data at substrate temperature 700 °C and various Ga effusion cell temperatures plotted by different symbols (a) during Ga adsorption and desorption and (b) during initial Ga deposition of 60 s. Solid lines show best fits to simple exponential decay and linear growth functions, respectively.

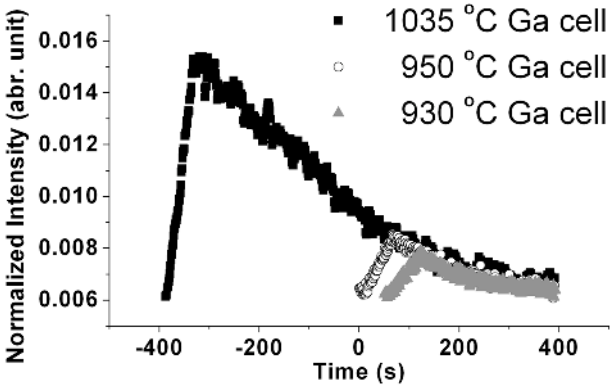

FIG. 12. (Color online) Plot of translated fluorescence data for a given substrate temperature at 700 °C.

by a simple exponential decay function, as shown in Fig. 10(a). Better fits can be obtained with simple models which assume that the desorption rate is proportional to droplet surface area and that all droplets have the same size. However, a model-independent approach is also possible. Figure 12 shows that the different desorption curves can be translated to lie on top of each other. This suggests that the desorption process is fundamentally the same for all cases despite the differences in initial Ga coverage.

2. Kinetics as a function of substrate temperature

Figure 13(a) shows the real-time Ga *K* fluorescence data during Ga adsorption and desorption at various substrate temperatures. The Ga flux was the same for all samples with a constant Ga cell temperature of 1035 °C. Figure 13(b) zooms in the initial Ga deposition of 60 s. The Ga effusion cell shutter was opened approximately 10 s after each scan started to obtain a base line for the signals. Following a transient, the adsorption process can again be fit by a linear function, and the relative slopes of the lines suggest a higher net adsorption rate at lower substrate temperatures. A plot of the adsorption rate as a function of substrate temperature is shown in Fig. 14. While we expect the net absorption process to have a potentially complex behavior because it involves both sticking coefficient and desorption rate [see Eq. (3) above], a simple Arrhenius fit of the substrate temperature dependence of the adsorption rate gives an effective activation energy of approximately 2.8 eV. This is quite similar to literature values of 2.88 eV reported for Ga adsorption on AlGaN.[17]

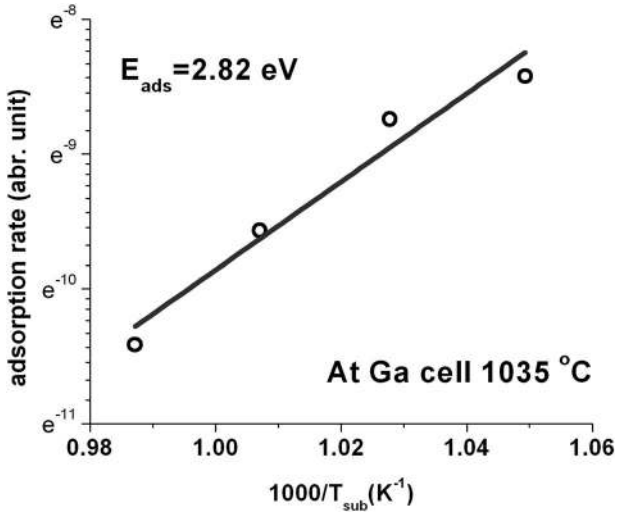

FIG. 14. Plot of net adsorption rates from linear fits as a function of sample substrate temperature.

We can estimate the temperature dependence of the sticking coefficient α. From Eq. (3) we expect that $\alpha = F^{-1}(A(t)+D(t))$. In fact, as noted above, in this regime the sticking coefficient is nearly constant in time because $A(t)$ is approximately constant in this regime and the temporal change in $D(t)$ is small relative to the size of $A(t)$. While the absolute flux F is not known, this approach allows the temperature dependence of the sticking coefficient to be calculated (Fig. 15).

Desorption occurs faster at higher substrate temperature. To quantify the effect we utilize the observation discussed above, i.e., that the desorption curves exhibit a strong similarity when shifted appropriately, suggesting that droplets pass through similar morphologies during desorption. We have found that the desorption curves at different substrate temperatures overlap after having been shifted as before, and then rescaled in time, as shown in Fig. 16(a). The rescaling factor then gives a relative rate of desorption at each substrate temperature. The relative desorption rates for different substrate temperatures are plotted in Fig. 16(b). The activation energy calculated is approximately 2.7 eV.

IV. DISCUSSION AND CONCLUSIONS

An important question that is not directly addressed here is the presence or absence of a Ga wetting layer on (0001) sapphire. Based upon XPS and LEED evidence Sidorenko *et*

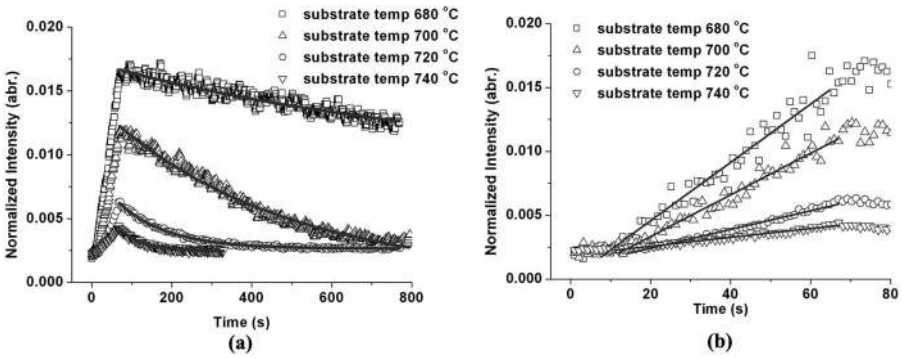

FIG. 13. Real-time Ga *K* fluorescence data at various substrate temperatures plotted by different symbols (a) during Ga adsorption and desorption and (b) during initial Ga deposition of 60 s. Solid lines show best fits as described in the text.

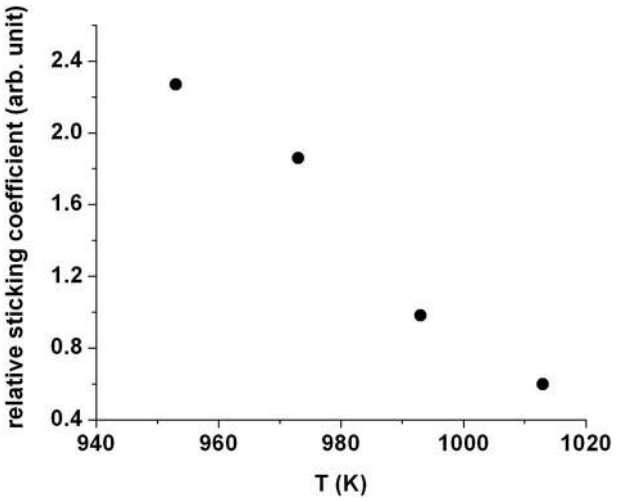

FIG. 15. Plot of relative sticking coefficient α as a function of sample substrate temperature.

al.[18] report that Ga does not form a wetting layer on (0001) sapphire, unlike the situation on GaN and SiC surfaces. We have found that, following nitridation of the droplets to form GaN nanodots, cross-section TEM shows a continuous 3-ML-thick GaN film wetting the surface for growth at 620 °C, but not at 680 °C.[15] The presence of a GaN film covering the surface following nitridation is consistent with Sidorenko *et al.*'s observation that Ga appears to spread from the droplets into the surrounding areas during the nitridation process. The energetics of the surface morphology are unclear. The surface energy of liquid Ga (about 0.69 J/m^2, Ref. 19) is much smaller than that of (0001) sapphire (approximately 2.0 J/m^2, Ref. 20) but we know of no measurements of the Ga/sapphire interfacial energy. More study of the presence or absence of a Ga wetting layer on sapphire is warranted.

In interpreting the overall desorption rate measured from the fluorescence data, it must be considered that it includes contributions from the droplets and the regions between them. On longer time scales than those shown in the figures, however, we find that the last stages of the Ga desorption process are very slow. This suggests that Ga atoms near the surface are more strongly bound than those in the bulk of the droplets and that the dominant desorption throughout the regime examined here is from the droplet surfaces. The activation energy measured here for desorption on sapphire is quite similar to that reported by other groups for the droplet regime on GaN and SiC. The value of 2.7 eV is close to the reported value of 2.76 eV for desorption from GaN in the (macroscopic) droplet regime by He *et al.*;[10] slightly larger than the value of 2.6 eV for Ga desorption from 6*H*-SiC(001) in the droplet regime reported by Zheng *et al.*[5] and less than the values of 3.1–3.2 eV for the droplet regime on GaN reported by Koblmäller *et al.*[6] All of these values are comparable to the Ga heat of vaporization, 2.7 eV/atom, as we might expect for evaporation from droplets. Overall, the similarity would suggest that the activation energy for desorption in the nanodroplet regime is not strongly sensitive to the substrate, though differences clearly exist for lower coverage levels.[11]

Theoretical models of droplet formation on surfaces[14,21–23] incorporate nucleation, coalesence, and ripening processes. If droplets nucleate homogeneously, it's expected that low deposition rates/high surface mobilities result in relatively fewer but larger droplets because adatoms are more likely to diffuse to existing droplets than to encounter other adatoms and nucleate a new droplet. Conversely, high deposition rates/lower surface mobilities are expected to give relatively more but smaller droplets. This is qualitatively consistent with the data of Tables I and II. However, it is noteworthy that, from the earliest time it is observable, the GISAXS peak due to droplet correlations moves toward smaller wavenumber. Thus, the time regime probed here is primarily dominated by droplet coarsening. The distribution of droplet sizes during the initial droplet formation process may be too broad to produce a well-defined peak in the GISAXS structure factor.

Simulations of Family and Meakin[14] of homogeneous droplet nucleation with growth and coalescence have shown the coexistence of monodispersed large droplets with polydispersed small droplets that form due to continuous nucleation. However, simultaneous heteregenous nucleation results only in a monodispersed distribution of droplets. In our related study of GaN nanodots formed by plasma nitridation of the droplets,[15] the surface morphology was examined *ex situ*. The AFM and TEM results of the GaN nanodot samples show a bimodal distribution of droplet sizes, which is in agreement with the simulation results from Family and Meakin for homogeneous nucleation, growth, and coalescence.

The most characteristic feature of the droplet ripening

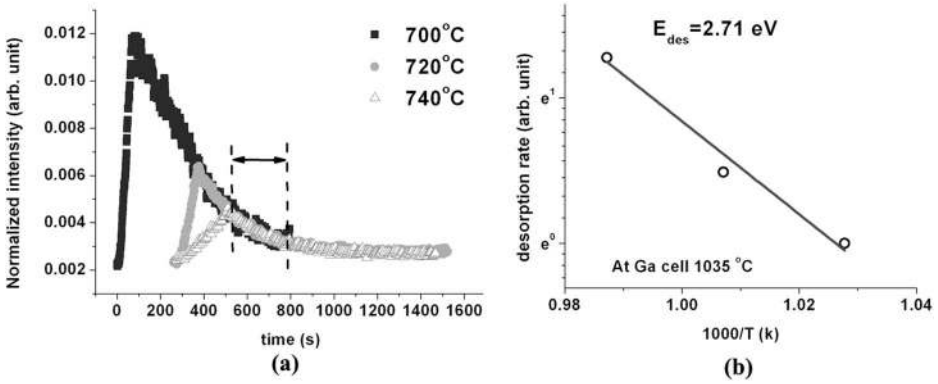

FIG. 16. (Color online) (a) Fluorescence data of different substrate temperatures after rescaling the time axis for each curve. (b) Plot of relative desorption rates given by the rescaling factors obtained from the overlap in (a).

process is the formation of a distribution of droplet sizes that evolves with time. As shown above, the GISAXS evolution exhibits dynamical scaling with a power law growth of the characteristic length scale during adsorption, in accord with expectations from the theory and simulations of Family and Meakin. The dimensionality of the droplets obtained from the power law fit is between that expected for two-dimensional (i.e., flat) and three-dimensional (i.e., spheroidal) droplets. This is consistent with a flattened spheroidal morphology.

In the Family–Meakin model coarsening occurs because of the coalescence of neighboring droplets that are growing due to the deposition. In this picture, the coarsening would stop in the absence of deposited atoms. However, we have observed continued coarsening of the correlation peak during desorption (Fig. 4), which must be due to a physical process not included in the Family–Meakin approach. It is unclear whether the dominant mechanism is preferential evaporation of smaller droplets on the surface, the transfer of atoms from smaller to larger droplets via surface diffusion, or movement of Ga droplets on the surface with subsequent impingement and coalescence.[11] We continue further studies to examine these issues in more detail.

ACKNOWLEDGMENTS

We would like to thank P. Siddons, R. France, and C. Sanborn for their help with the experiments. We would also like to thank Dr. N. Bouet and Professor T.D. Moustakas for valuable discussions. This work was partially supported by DOE DE-FG02-03ER46037 and NSF DMR-0507351. The real-time x-ray system for surface processes was made possible by NSF DMR-0114154 and NSF DMR-0116567. "Data for this study were measured at beamline X21 of the National Synchrotron Light Source (NSLS). Financial support comes principally from the Offices of Biological and Environmental Research and of Basic Energy Sciences of the US Department of Energy."

[1] E. J. Tarsa, B. Heying, X. H. Wu, P. Fini, S. Den Baars, and J. S. Speck, J. Appl. Phys. **82**, 5472 (1997).
[2] B. Heying, R. Averbeck, L. F. Chen, E. Haus, H. Riechert, and J. S. Speck, J. Appl. Phys. **88**, 1855 (2000).
[3] B. Heying, I. Smorchkova, C. Poblenz, C. Elsass, P. Fini, S. DenBaars, U. Mishra, and J. S. Speck, Appl. Phys. Lett. **77**, 2885 (2000).
[4] J. E. Northrup and J. Neugebauer, Phys. Rev. B **60**, R8473 (1999).
[5] L. X. Zheng, M. H. Xie, and S. Y. Tong, Phys. Rev. B **61**, 4890 (2000).
[6] G. Koblmuller, R. Averbeck, H. Riechert, and P. Pongratz, Phys. Rev. B **69**, 035325 (2004).
[7] C. Adelmann, J. Brault, D. Jalabert, P. Gentile, H. Mariette, G. Mula, and B. Daudin, J. Appl. Phys. **91**, 9638 (2002).
[8] M. McLaurin, B. Haskell, S. Nakamura, and J. S. Speck, J. Appl. Phys. **96**, 327 (2004).
[9] S. Guha, N. A. Bojarczuk, and D. W. Kisker, Appl. Phys. Lett. **69**, 2879 (1996).
[10] L. He, Y. T. Moon, J. Xie, M. Muñoz, D. Johnstone, and H. Morkoç, Appl. Phys. Lett. **88**, 071901 (2001).
[11] A. S. Ozcan, Y. Wang, G. Ozaydin, K. F. Ludwig, A. Bhattacharyya, T. D. Moustakas, and D. P. Siddons, J. Appl. Phys. **100**, 084307 (2006).
[12] S. K. Sinha, E. B. Sirota, S. Garoff, and H. B. Stanley, Phys. Rev. B **38**, 2297 (1998).
[13] M. Born and E. Wolf, *Principles of Optics* (Cambridge University Press, Cambridge, 1980).
[14] F. Family and P. Meakin, Phys. Rev. A **40**, 3836 (1989).
[15] Y. Wang, A. S. Ozcan, C. Sanborn, K. F. Ludwig, A. Bhattacharyya, R. Chandrasekaran, T. D. Moustakas, L. Zhou, and D. Smith, J. Appl. Phys. **102**, 073522 (2007).
[16] R. E. Honig and D. A. Kramer, RCA Rev. **30**, 285 (1969).
[17] E. Iliopoulos and T. D. Moustakas, Appl. Phys. Lett. **81**, 295 (2002).
[18] A. Sidorenko, H. Peisert, H. Neumann, and T. Chassé, Surf. Sci. **601**, 4521 (2007).
[19] S. C. Hardy, J. Cryst. Growth **71**, 602 (1985).
[20] J. R. Smith and W. Zhang, Acta Mater. **48**, 4395 (2000).
[21] A. Pimpinelli and J. Villain, *Physics of Crystal Growth* (Cambridge University Press, Cambridge, 1999).
[22] J. A. Blackman and S. Brochard, Phys. Rev. Lett. **84**, 4409 (2000).
[23] S. Ulrich, S. Stoll, and E. Pefferkorn, Langmuir **20**, 1763 (2004).